Advances in Aerospace Science and Technology, 2025, 10(2), 52-63
https://www.scirp.org/journal/aast
ISSN Online: 2473-6724
ISSN Print: 2473-6708

Aerodynamic Characteristics Analysis of Takeoff Transition Mode for Tilting Wing Unmanned Aerial Vehicles at Different Pitch Angles

Kaixu Zhang, Guoyi He, Chengbo Peng, Zhile Hong

Academy of Aeronautics and Astronautics, Nanchang Hangkong University, Nanchang, China
Email: hegy509@163.com

How to cite this paper: Zhang, K.X., He, G.Y., Peng, C.B. and Hong, Z.L. (2025) Aerodynamic Characteristics Analysis of Takeoff Transition Mode for Tilting Wing Unmanned Aerial Vehicles at Different Pitch Angles. *Advances in Aerospace Science and Technology*, **10**, 52-63.
https://doi.org/10.4236/aast.2025.102004

Received: March 10, 2025
Accepted: June 24, 2025
Published: June 27, 2025

Abstract

The tilting wing UAV, as a tilting powered vertical takeoff and landing aircraft with both vertical takeoff and landing and high-speed cruise capabilities, can flexibly switch between helicopter mode and fixed wing mode. In the tilt transition mode, parameters such as flight attitude angle, forward flight speed, and tilt speed will continue to dynamically change with the change of tilt angle. The multi-degree-of-freedom coupling effect leads to strong unsteady aerodynamic characteristics of the entire machine. The dynamic characteristics of multi-parameter strong coupling pose a severe challenge to the control stability of aircraft and become a difficult point in the design of tilt wing unmanned aerial vehicle control systems. This article uses the unsteady momentum source method to numerically calculate and analyze the takeoff transition modes of a tilting wing unmanned aerial vehicle at a tilt speed of 20˚/s, uniform acceleration inflow, and 0˚, −2˚, and −5˚ pitch angles. In order to grasp their aerodynamic interference laws and provide reference for the design and control theory research of such aircraft.

Keywords

The Tilting Wing UAV, Unsteady Momentum Source Method, Transition Mode, Aerodynamic Analysis

1. Introduction

Vertical takeoff and landing fixed wing aircraft combine the advantages of fixed wing aircraft in range, endurance, and cruising speed with the vertical takeoff and landing capabilities of helicopters, forming a unique comprehensive performance advantage with broad application prospects [1] [2]. Vertical takeoff and landing fixed wing aircraft do not rely on runways and can achieve precise fixed-point takeoff and hovering, especially suitable for deck takeoff and landing, rapid takeoff and landing, and situations without runways, greatly enhancing the ability to perform special tasks [3] [4]. Its unique structural layout and power transmission system enable vertical takeoff and landing aircraft to adapt to a wide range of military and civilian applications. It has become a key research object in the aviation industry and demonstrates the development trend of future aircraft technology [5].

Vertical takeoff and landing fixed wing unmanned aerial vehicles have various configurations with different technical characteristics, mainly divided into three types: tailstock, lift push composite, and tilt power.

Despite the superior performance and larger flight envelope of tiltrotor aircraft, there are many important challenges in their own configuration that have not been effectively resolved. In helicopter mode, the downwash flow of the rotor is obstructed by the wing and forced to flow along the wing spanwise direction, squeezing each other at the symmetrical plane of the wing and spraying upwards, forming its unique "fountain effect"; At the same time, due to the continuous impact of the downwash flow of the rotor on the wing, the "weight gain effect" results in a decrease in its carrying capacity. In hover, the maximum loss of rotor pulling force can reach 15% [6]; When descending vertically, a tiltrotor aircraft is prone to enter a vortex state, causing the aircraft to lose control. In transition mode, the speed range of the tiltrotor aircraft is too narrow, which can easily lead to control errors; During transition mode and high-speed forward flight, it is easy to encounter aeroelastic stability problems caused by the coupling between the rotor and wing, as well as flutter problems caused by rotor rotation [7].

Tilting wing unmanned aerial vehicles effectively solve the problem of tension loss caused by rotor downwash flow and the generation of "fountain effect". However, in transition mode, due to the coupling of various factors such as rotor slip flow, forward flow, and rotor dynamic tilt process, the aerodynamic characteristics under tilt transition have strong nonlinear and unsteady characteristics. The aerodynamic characteristics of tilt wing unmanned aerial vehicles in transition mode affect the design of flight control systems and the strength design of tilt mechanisms to varying degrees, and have a significant impact on the stability and reliability of unmanned aerial vehicles. Therefore, the study of aerodynamic characteristics of tilt wing unmanned aerial vehicles in transition mode is particularly important.

2. Models and Methods

2.1. Geometric Model and Parameter

The tilting wing unmanned aerial vehicle model used for calculation in this article is shown in **Figure 1**. The flight state of the tilting wing unmanned aerial vehicle at low Reynolds numbers does not require a power device. The overall weight of the tilting wing unmanned aerial vehicle is relatively light, with a total weight of 3 kg and a body length of 1 m [8]. It does not require high-power motors to output power at low speeds. Therefore, a motor with small space occupation and a regular shape can be selected. This small motor installed on the tilting wing unmanned aerial vehicle has little impact on the overall flow field, so the presence of the motor is ignored in modeling to ensure that the aerodynamic shape of the tilting wing unmanned aerial vehicle is not affected. The calculation method used in this article is the momentum source method, which does not require the establishment of a real model of the rotor. Therefore, when establishing the overall model of the rotor, a working disk with the rotor spans as the radius is established at the position where the rotor is located (half the span of the tilting wing).

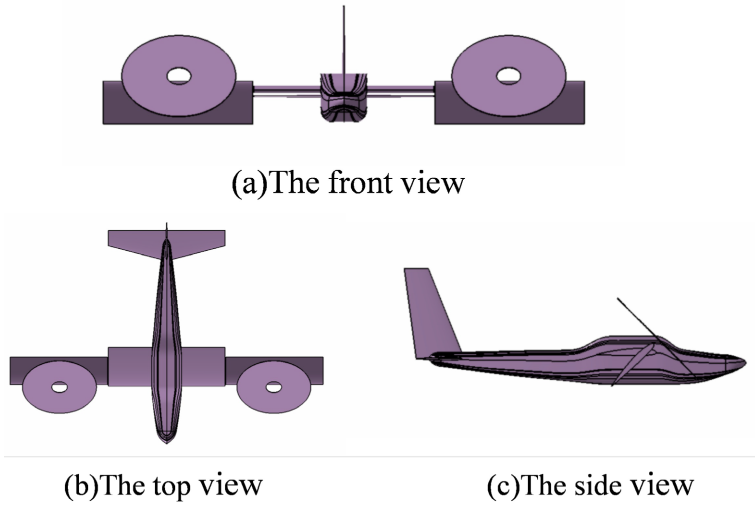

Figure 1. The tilting wing unmanned aerial vehicle model.

The wing parameters are shown in **Table 1**:

Table 1. The wing parameters.

Parameter	Numerical value
Wing type model	NACA2412
Wing chord length (m)	0.2
Wing installation angle (˚)	2
Half machine model fixed wingspan length (m)	0.3
Half machine model tilting wingspan length (m)	0.5
Tilt angle (˚)	86

2.2. Maintaining the Integrity of the Specifications

The derivation of the momentum source term, as shown in **Figure 2**, for a certain element on the propeller disk, its distance from the center of the propeller disk is r, the radial length of the blade element is dr, and the circumferential length is $r\Delta\phi$.

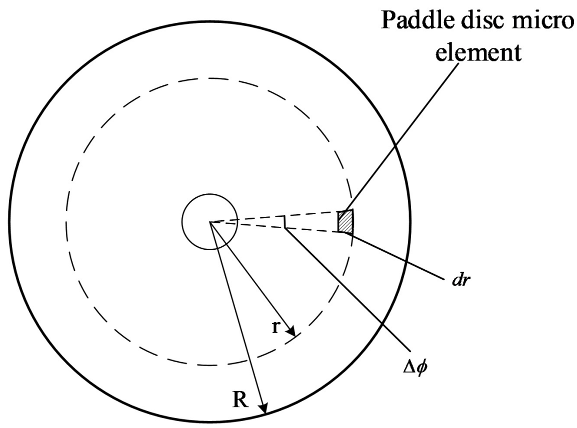

Figure 2. The derivation of the momentum source term.

The rotor speed is Ω, and the time it takes for a single blade to make one complete revolution is t_0 as follows:

$$t_0 = \frac{2\pi}{\Omega} \tag{1}$$

In a circular mesh, the central angle occupied by a single mesh is $\Delta\phi$. The time required for a single piece to rotate through one grid per unit time $t_{d\phi}$ is as follows:

$$t_{d\phi} = \frac{\Delta\phi}{\Omega} \tag{2}$$

According to Newton's third law, the magnitude of the action and reaction forces is equal and the direction is opposite. The force exerted on the blade element by the airflow is $d\vec{F}$, the force exerted by the blade element on the airflow is $-d\vec{F}$. If the effect of the force of the blade element on the airflow in one cycle is equivalent to that of the grid element, then the force of a single blade on the grid element per unit time dF_r is as follows:

$$dF_r = -dF \cdot \frac{\Delta\phi}{\Omega} \cdot \frac{\Omega}{2\pi} = -dF \cdot \frac{\Delta\phi}{2\pi} \tag{3}$$

In the structural grid of the propeller disc, a sector-shaped region that dynamically changes over time is used instead of the actual blade motion, and the addition of a non-stationary momentum source term is determined based on the blade position. To ensure that there is no situation of sweeping half of the grid, it is necessary to set the time step at the corresponding speed, that is, only one grid cell is swept in each time step. Therefore, the unsteady momentum source term is as follows:

$$F_\Delta = \frac{\Delta\phi}{\Omega\Delta t} \cdot \left(-dF_r\right) \cdot \frac{1}{V_c} = \left(-dF_r\right) \cdot \frac{1}{V_c} \tag{4}$$

This article selects the flow field of a single rotor with NACA0012 as the airfoil in hovering state as the research object, and compares the calculated results with the experimental data provided by McKee J W [9]. The specific modeling parameters of the rotor are shown in **Table 2**. (**Figure 3**)

Table 2. Specific parameters of the rotor.

Parameter	Numerical value
Wing type model	NACA0012
Wing chord length (m)	0.2
Wing installation angle (˚)	2
Half machine model fixed wingspan length (m)	0.224
Half machine model tilting wingspan length (m)	0.5
Tilt angle (˚)	86

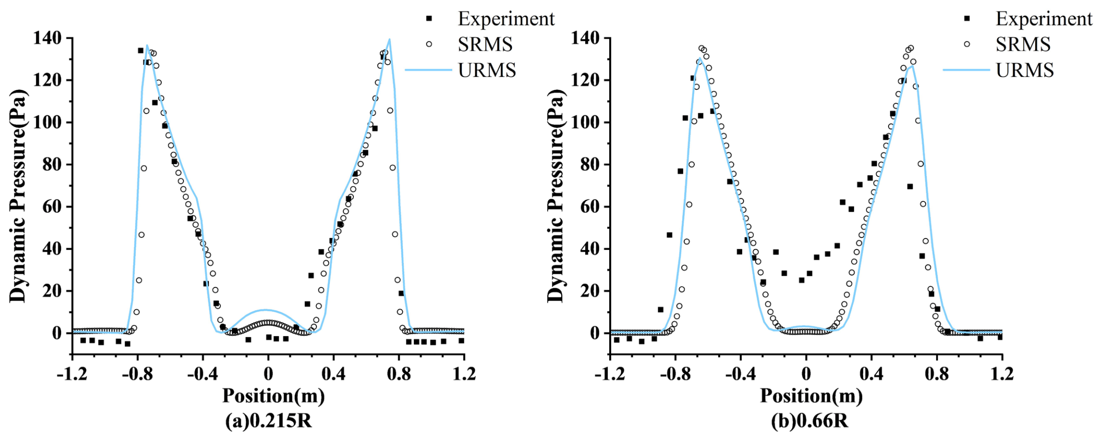

Figure 3. The derivation of the momentum source term.

3. Calculation Results and Discussion

Due to the lack of consideration for the lateral and lateral aerodynamic characteristics of the drone in the calculation, and the fact that the calculation model is a symmetrical model, a half aircraft model of a tilting wing drone is used to reduce computational complexity and improve efficiency.

3.1. Calculation Conditions

The tilting wing drone accelerates during takeoff transition mode. Due to the focus of this study on investigating the impact of pitch angle changes on the aerodynamic characteristics of a tilting wing unmanned aerial vehicle during takeoff transition mode, the tilting strategy and dynamic balance of the tilting wing unmanned aerial vehicle are not studied. Therefore, the takeoff transition mode is simplified as a uniform acceleration process, and the force balance problem of the tilting wing unmanned aerial vehicle is not considered in the calculation process. The range of downflow velocity variation in takeoff transition mode is 0 m/s - 23 m/s, the inflow acceleration at the inlet is 5.34883721 m/s^2, the rotor speed is a constant value of 580 rad/s, and the tilt speed is 20˚/s for uniform tilt. The study was conducted on the pitch angles of the entire aircraft at 0˚, −2˚, and −5˚. The tilt angle is the angle between the tilt wing and the axis of the fuselage, independent of the pitch angle. During forward flight at different pitch angles, the actual angle of attack of the tilt wing is the sum of the tilt angle and the pitch angle.

3.2. Comparison of Calculation Results

As shown in **Figures 4-6**, the lift and drag curves of the continuous tilt calculation results are presented for pitch angles of 0˚, −2˚, and −5˚, respectively. In the figure, the rotor tension is measured using the sliding grid method at a fixed tilt angle, and the lift and drag forces are measured using the unsteady momentum source method for the lift and drag generated by the tilting wing, fixed wing, and fuselage.

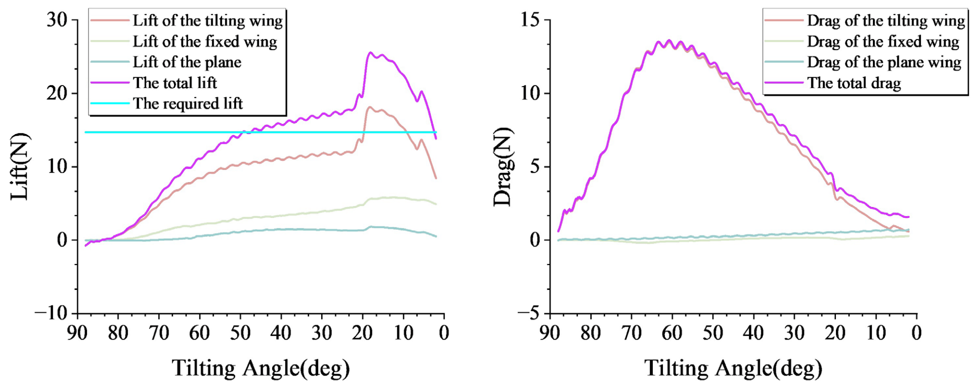

Figure 4. Lift and drag at 0˚ pitch angle.

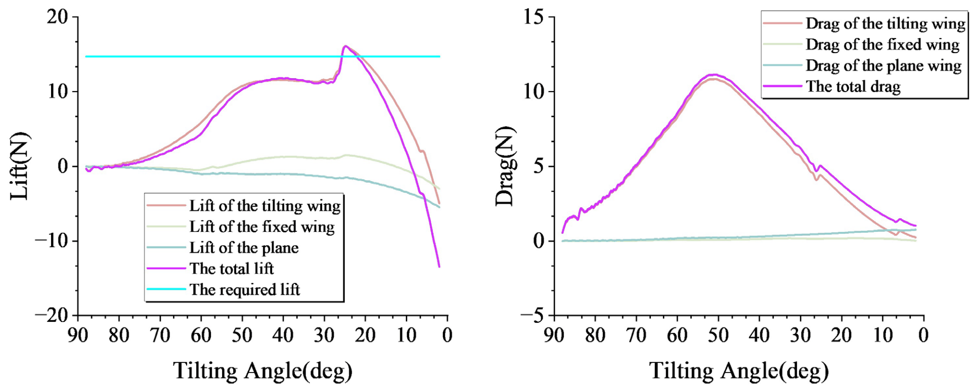

Figure 5. Lift and drag at −2˚ pitch angle.

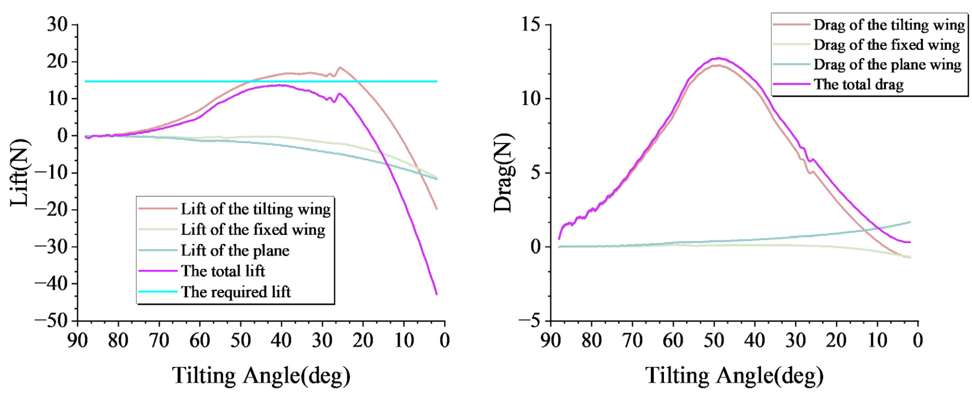

Figure 6. Lift and drag at −5˚ pitch angle.

As can be seen from **Figure 4**:

1) The lift is mainly generated by the tilting wing and the fixed wing together, and the change trend of the resultant lift force is basically consistent with that of the tilting wing. Between tilting angles of 88˚ and 80˚, except for the rotor, each component of the UAV basically does not generate lift. Between tilting angles of 80˚ and 20˚, the lift of the fixed wing gradually increases as the tilting angle decreases, with a basically constant growth rate. Between tilting angles of 80˚ and 60˚, the lift of the tilting wing gradually increases at a faster growth rate. Between tilting angles of 60˚ and 20˚, the lift tends to be gentle, with only a slight increase. Near a tilting angle of 20˚, the lift of the tilting wing experiences a sudden increase and reaches its peak at a tilting angle of 17˚. As the tilting angle continues to decrease, the lift of the tilting wing gradually decreases. The growth rate of the fixed wing's lift at a 20˚ tilting angle shows corresponding changes with the tilting wing's lift, but it does not significantly decrease as the tilting angle continues to decrease. Near a tilting angle of 5˚, the lift of the tilting wing slightly rebounds and then continues to decrease. The lift of the fuselage remains basically near 0 throughout the tilting process.

2) Drag mainly originates from the tilting wing. Between tilting angles of 88˚ and 60˚, the drag increases significantly and reaches its peak near a tilting angle of 60˚. As the tilting angle continues to decrease, the drag gradually decreases. The fixed wing and fuselage basically do not generate drag.

As can be seen from **Figure 5**:

1) Between tilting angles of 88˚ and 80˚, the UAV basically generates no lift. Between tilting angles of 80˚ and 60˚, the fuselage and fixed wing produce negative lift and maintain a downward trend. Although the negative lift value is small, within this range, the resultant lift force is significantly lower than the tilting wing lift. Between tilting angles of 60˚ and 20˚, the fixed wing generates lift and gradually increases, counteracting the fuselage's negative lift, making the resultant lift force consistent with the tilting wing lift. Near a tilting angle of 25˚, the tilting wing lift increases significantly and reaches its peak at a tilting angle of 20˚; the fixed wing lift also increases slightly. As the tilting angle continues to decrease, the lift of the tilting wing, fixed wing, and fuselage all decline continuously. Near a tilting angle of 10˚, the resultant lift force becomes negative.

2) Drag mainly originates from the tilting wing, while the fixed wing generates less drag, and the fuselage basically produces no drag. Between tilting angles of 88˚ and 50˚, the tilting wing drag and resultant drag force gradually increase and basically coincide, reaching their peaks near a tilting angle of 50˚. As the tilting angle continues to decrease, the drag gradually decreases but remains positive throughout.

As can be seen from **Figure 6**:

1) Between tilting angles of 88˚ and 75˚, the UAV basically generates no lift. In the subsequent tilting process, both the fixed wing and fuselage produce negative lift, and the negative lift increases as the tilting angle continues to decrease. Be-

tween tilting angles of 75˚ and 60˚, the growth rate of the tilting wing lift and the resultant lift force is slow. Between tilting angles of 60˚ and 40˚, the tilting wing lift grows at a relatively large rate, and the resultant lift force reaches its maximum value near a tilting angle of 40˚. Between tilting angles of 40˚ and 25˚, the tilting wing lift remains basically unchanged, while the resultant lift force gradually decreases. Near a tilting angle of 25˚, the resultant lift force slightly increases, corresponding to a small peak in the tilting wing lift, but the resultant lift force at this point is smaller than the maximum lift and can no longer be called a peak. As the tilting angle continues to decrease, both the tilting wing lift and the resultant lift force show a rapid downward trend. Near a tilting angle of 20˚, the resultant lift force becomes negative, and when the tilting is complete, the resultant lift force is approximately −40 N.

2) The drag of the fixed wing and fuselage exhibits a reverse variation trend: the fuselage drag gradually increases, while the fixed wing produces negative drag. The tilting wing drag and the resultant drag force show a variation trend similar to that at a pitch angle of −2˚ under this pitch angle, but near a pitch angle of 10˚, the tilting wing exhibits negative drag, while the resultant drag force does not become negative.

3.3. Analysis of Calculation Results

The combined force of lift and drag mainly comes from the tilting wings, and the fuselage and fixed wings are not affected by rotor slipstream. Draw the comparison between lift and drag of the tilting wing as shown in **Figure 7**:

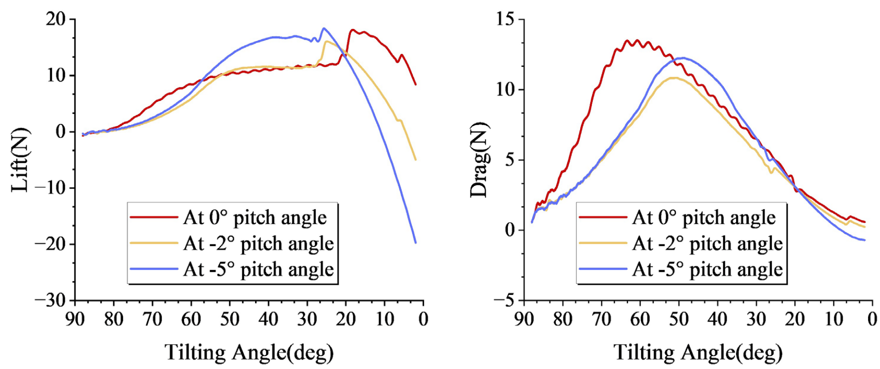

Figure 7. Comparison of lift and drag of tilting wings at different pitch angles.

The differences in lift can be divided into three stages: before a tilting angle of 60˚, the lift at a 0˚ pitch angle is greater than that at negative pitch angles; between tilting angles of 60˚ and 20˚, the tilting wing lift is the largest at a −5˚ pitch angle, while the tilting wing lift at 0˚ and −2˚ pitch angles remains basically consistent; between tilting angles of 20˚ and 2˚, the lift decreases sequentially as the pitch angle decreases. Additionally, the tilting angle corresponding to the tilting wing lift peak gradually increases with the decrease of the pitch angle, but the lift peak values at 0˚ and −5˚ pitch angles are similar and larger than that at a −2˚ pitch angle.

In terms of drag, between tilting angles of 88˚ and 50˚, the tilting wing drag at a 0˚ pitch angle is significantly larger than that at negative pitch angles; between tilting angles of 50˚ and 20˚, the drag at a −5˚ pitch angle is slightly larger, while the drag at a −2˚ pitch angle is the smallest; between tilting angles of 20˚ and 2˚, the drag decreases sequentially as the pitch angle decreases.

Figures 8-10 show the streamlines and pressure nephograms at the middle position of the tilting wing (the center of the rotor) under pitch angles of 0˚, −2˚, and −5˚, respectively. At the same tilting angle, the rotors in each figure are rotated to the same position, so there is no influence of blade azimuth angle differences on the pressure distribution.

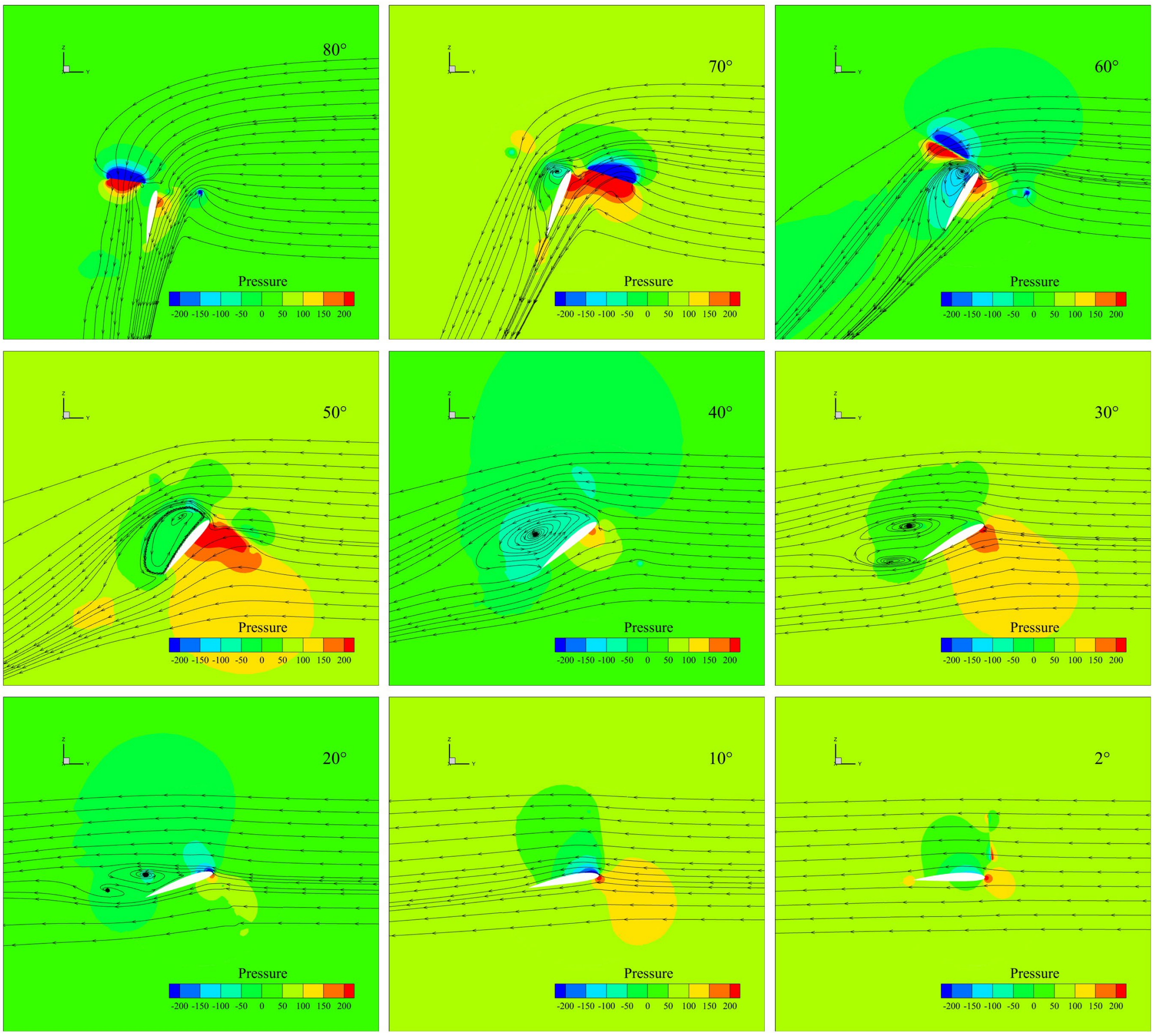

Figure 8. Pressure and streamline diagram at 0˚ pitch angle.

By comparing the pressure contour plots at tilting angles from 80˚ to 60˚, it can be observed that: at a pitch angle of 0˚, a significant negative pressure region appears on the upper surface of the tilting wing UAV, whereas no obvious negative pressure region is found at negative pitch angles. In contrast, similar positive pressure regions are observed on the lower surface of the tilting wing under all pitch angles. Therefore, at a pitch angle of 0˚, a larger pressure difference between the upper and lower surfaces of the tilting wing generates greater lift. Comparison of the pressure distributions at a tilting angle of 50˚ reveals that: when the pitch angle is 0˚, the lower surface exhibits the highest positive pressure while the upper surface shows relatively small negative pressure; when the pitch angle is −5˚, although the lower surface pressure is slightly lower than that at 0˚ pitch, the upper surface develops a larger negative pressure region with higher magnitude, resulting in a greater pressure differential and thus larger lift force.

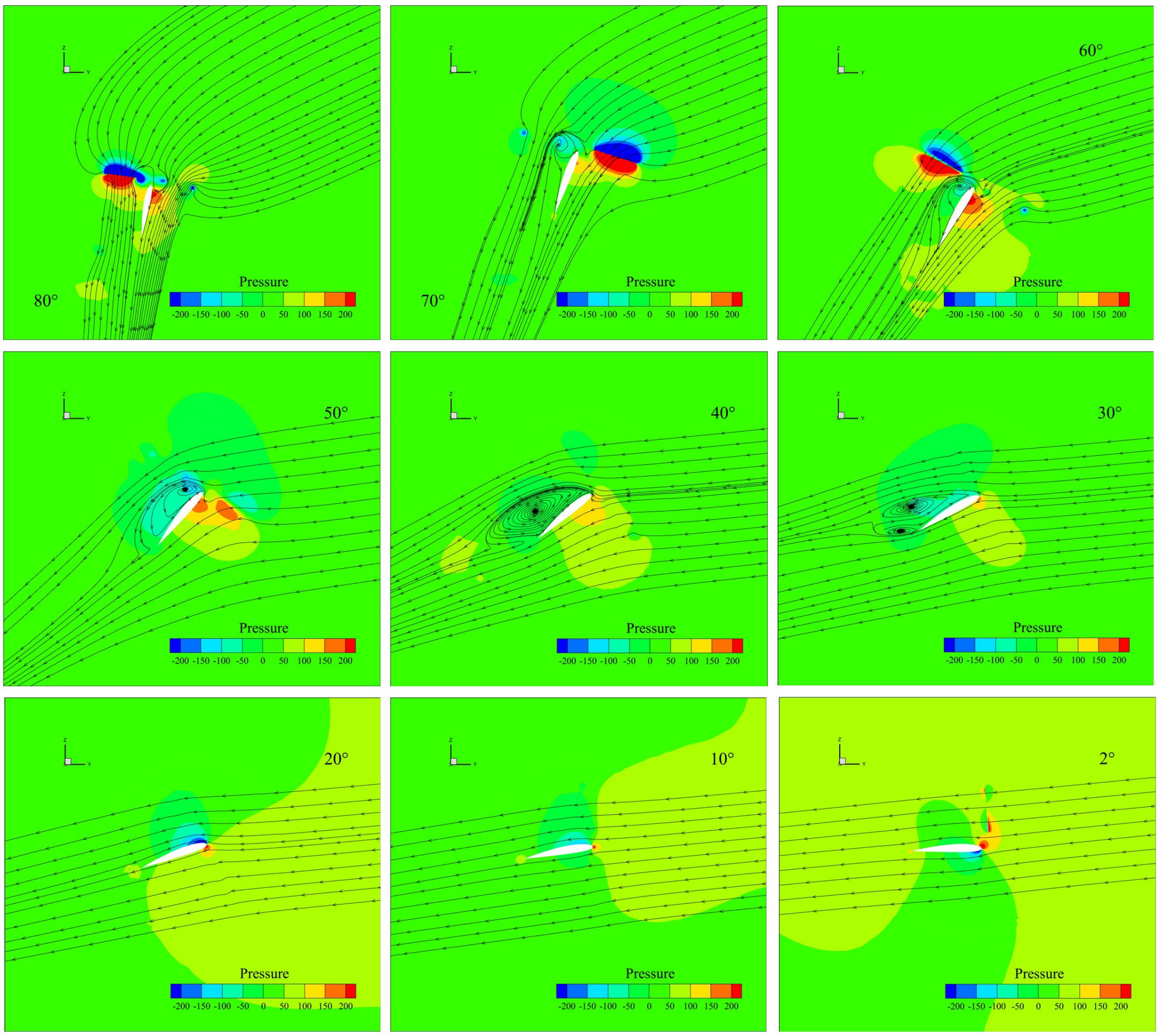

Figure 9. Pressure and streamline diagram at −2˚ pitch angle.

As shown in **Figure 8**, at a pitch angle of 0˚, the airflow over the tilting wing transitions from separated flow to attached flow between tilting angles of 20˚ and 10˚, which corresponds to the tilting angle range where the lift peak occurs in **Figure**

7. Similarly, in **Figure 9** and **Figure 10**, at pitch angles of −2˚ and −5˚, the flow transition from separation to attachment occurs between 30˚ and 20˚ of tilting angle, coinciding with the lift peak regions. This indicates that during the takeoff transition mode, the flow transition from separated to attached flow over the tilting wing causes a sudden increase in lift, followed by a gradual decrease as the tilting angle further decreases.

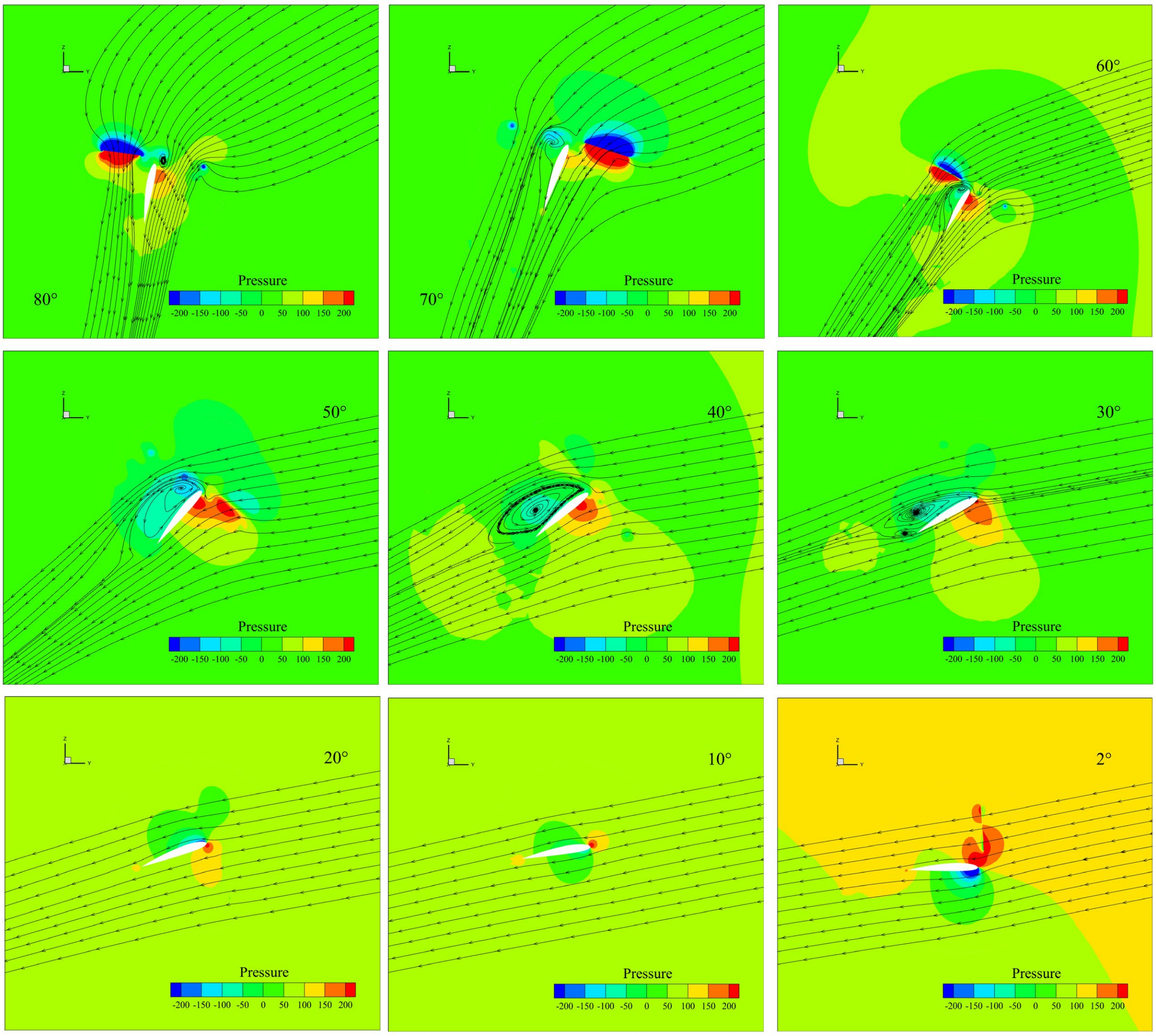

Figure 10. Pressure and streamline diagram at −5˚ pitch angle.

4. Conclusion

At a pitch angle of 0˚, the resultant lift force exhibits better performance. During the mid-stage of wing tilting, the required lift for the UAV can be fully provided by the wing without relying on the rotor thrust component; however, the lift fluctuation amplitude reaches its maximum during the airflow transition process. When the UAV flies forward at negative pitch angles, the lift generated by the wing and fuselage alone is insufficient to meet the required lift, necessitating an increased rotor speed to provide additional lift. At a pitch angle of 0˚, higher drag is generated during the initial tilting phase, whereas a pitch angle of −2˚ consistently yields the lowest overall drag. After the tilting angle reaches 50˚, the drag difference between 0˚ and −2˚ pitch angles gradually decreases. Therefore, during the initial tilting phase of the takeoff transition mode, a pitch angle of −2˚ is recommended for forward flight, and the pitch angle should be adjusted back to 0˚ during the mid-tilting stage.

Conflicts of Interest

The authors declare no conflicts of interest regarding the publication of this paper.

References

[1] Wei, Z.P., Liu, F. and Yang, S. (2024) Development and Key Technologies of Vertical Take-Off and Landing UAV with Fixed Wing. *Aircraft Design*, **44**, 5-13.

[2] Wang, K.L., Zhou, Z., Ma, Y.W., Du, W.S., Guo, J.H. and Li, X. (2022) Vertical Take-Off and Landing Fixed-Wing UAV Technology Development and Trend Analysis. *Advances in Aeronautical Engineering*, **13**, 1-13.

[3] Yu, J.Y. and Wang, C. (2017) Development Status and Prospects of Vertical Takeoff and Landing Unmanned Aerial Vehicle Technology. *Aerodynamic Missile*, **5**, 37-42.

[4] Chen, A.Q., Cui, J.D., Yang, Z.P., Tian, H. and Gao, J.L. (2021) Development and Inspiration of the Pre-Research Project for High Speed Vertical Takeoff Aircraft in the United States. *Aerodynamic Missile Journal*, **1**, 91-98.

[5] Zhu, C.L., Yuan, C. and Yang, J.H. (2022) Review of Foreign Military UAV Equipment Technology Development in 2021. *Tactical Missile Technology*, **1**, 38-45.

[6] Guo, J.D. and Song, Y.G. (2015) Testing Study on Aerodynamics and Control Characteristics of a Small Unmanned Tilt Rotor. *Acta Aerodynamica Sinica*, **33**, 107-112.

[7] Xu, M. (2003) Overview of the Development and Key Technologies of Tiltrotor Aircraft. *Helicopter Technique*, **2**, 40-44.

[8] Wang, Y.C., He, G.Y. and Wang, Q. (2022) Aerodynamic Performance Analysis and Optimization of Tilt-Wing UAV in Return Transition Section. *Science Technology and Engineering*, **22**, 9848-9856.

[9] McKee, J.W. and Naeseth, R.L. (1958) Experimental Investigation of the Drag of Flat Plates and Cylinders in the Slipstream of a Hovering Rotor. NASA Technical Reports Server.